Structural Difference between Group I and Group II Cobra Cardiotoxins: X-ray, NMR, and CD Analysis of the Effect of *cis*-Proline Conformation on Three-Fingered Toxins†

Ting-Shou Chen,‡ Fong-Yu Chung,‡,§ Siu-Cin Tjong,‡ King-Siang Goh,‡ Wei-Ning Huang,‡ Kun-Yi Chien,‡ Po-Long Wu,‡ Hua-Ching Lin,|| Chun-Jung Chen,*,§,⊥ and Wen-guey Wu*,‡

Institute of Bioinformatics and Structural Biology, National Tsing Hua University, Hsinchu 300, Taiwan, Biology Group, Research Division, National Synchrotron Radiation Research Center, Hsinchu 300, Taiwan, Department of Physics, National Tsing Hua University, Hsinchu 300, Taiwan, and Department of Zoology, Taipei Zoo, Taipei 116, Taiwan

Received January 28, 2005; Revised Manuscript Received March 21, 2005

ABSTRACT: Natural homologues of cobra cardiotoxins (CTXs) were classified into two structural subclasses of group I and II based on the amino acid sequence and circular dichroism analysis, but the exact differences in their three-dimensional structures and biological significance remain elusive. We show by circular dichroism, NMR spectroscopic, and X-ray crystallographic analyses of a newly purified group I CTX A6 from eastern Taiwan cobra (*Naja atra*) venoms that its loop I conformation adopts a type VIa turn with a cis peptide bond located between two proline residues of PPxY. A similar "banana-twisted" conformation can be observed in other group I CTXs and also in cyclolinopeptide A and its analogues. By binding to the membrane environment, group I CTX undergoes a conformational change to adopt a more extended hydrophobic domain with β-sheet twisting closer to the one adopted by group II CTX. This result resolves a discrepancy in the CTX structural difference reported previously between solution as well as crystal state and shows that, in addition to the hydrophobicity, the exact loop I conformation also plays an important role in CTX−membrane interaction. Potential protein targets of group I CTXs after cell internalization are also discussed on the basis of the determined loop I conformation.

Cardiotoxins (CTXs), the major toxin component that constitutes ~50% of total cobra venom, are all β-sheet, basic polypeptides of 60−62 amino acid residues with a three-fingered loop folding topology (*1*). Because of the amphiphilic property of CTX molecules and the well-established CTX action that causes systolic heart arrest by depolarizing cardiomyocytes, the previous study of its structure−function relationship has been mainly devoted to identifying the biological target responsible for the CTX-induced extra conductance of cell membranes (*2*). We have recently shown that membrane lipid-induced oligomerization of CTX, followed by membrane pore formation (*3*), is the most likely mechanism responsible for the CTX-induced influx of extracellular calcium. For the CTX-induced tissue degeneration (*4*), integrin may also be involved in the process (*5*). The complex mechanism of the CTX-induced toxicity indicates the presence of biological subclasses.

Evidence based on the structure−function correlation studies indeed indicates the diversity of CTX. First, on the basis of the interaction strength of CTX with zwitterionic sphingomyelin vesicles, CTX of two types, P and S, can be classified according to the hydrophobicity of the amino acids near the tip of loop II and the availability of Pro30 in that region (*6*). Second, depending on the presence of specific basic amino acid residues, CTX can also be classified according to their glycosaminoglycan binding ability responsible for its cell retention behavior (*7*). Finally, comparative analysis of CTX using circular dichroism (CD), immunological techniques, and secondary structure prediction indicates the presence of two other structural subclasses, i.e., groups I and II (*8*). Alignment of amino acid sequences of studied CTXs indicates that all group I CTXs, including toxin γ (Tγ) from *Naja nigricollis*, consist of a conserved sequence of LIPPF near the tip of loop I (Table 1; see also refs *9*−*21*). The observed differences were suggested to result from twisting curvatures of differing degree in the antiparallel β-sheet, which constitutes the main secondary structure of CTX.

In this study, we purify newly identified group I CTX A6 (*22*−*24*) from cobra venom of eastern Taiwan. Structural and dynamic analysis of CTX A6 through CD, NMR, and X-ray methods indicates that its loop I conformation in both solution and the crystal state adopts a type VIa turn with a cis peptide located between two proline residues of PPxY, a class I WW binding motif. The "banana-twisted" conformation of group I CTX at the loop I region exhibits a striking

† This work was funded by National Science Council Grant NSC-91-2113-M-007-041 to W.W. and Grants NSC-90-2321-B-213-001 and NSRRC 914RSB02 to C.-J.C.

* To whom correspondence should be addressed. W.W.: Institute of Bioinformatics and Structural Biology, National Tsing Hua University, Hsinchu 300, Taiwan; telephone, 886-3-573-1040; fax, 886-3-571-5934; e-mail, wgwu@life.nthu.edu.tw. C.-J.C.: Biology Group, Research Division, National Synchrotron Radiation Research Center, Hsinchu 300, Taiwan; telephone, 886-3-578-0281 ext. 7330; fax, 886-3-578-3813; e-mail, cjchen@nsrrc.org.tw.

‡ Institute of Bioinformatics and Structural Biology, National Tsing Hua University.

§ National Synchrotron Radiation Research Center.

|| Taipei Zoo.

⊥ Department of Physics, National Tsing Hua University.

10.1021/bi050172e CCC: $30.25
Published on Web 04/30/2005

Table 1: Sequences of CTX Homologues with Three-Dimensional Structures Determined by NMR and/or X-ray Analysis

Class	CTX	10	20	30	40	50	60	Method	pH	Temp.	Code	Reference
I	A6	LKC NQLIPPF	YKTCAAGKNL	CYKMFMVAAP	KVPVKRGCID	VCPKSSLLVK	YVCCNTDRCN	X-ray (1.6 Å)	6.8	110K[§]	1UG4	*This work*
	M1	LKC NQLIPPF	WKTCPKGKNL	CYKMTMRAAP	MVPVKRGCID	VCPKSSLLIK	YMCCNTNKCN	NMR	3.6	318K	2CCX	O'Connell *et. al.* (9)
	M2	LKC NQLIPPF	WKTCPKGKNL	CYKMTMRGAS	KVPVKRGCID	VCPKSSLLIK	YMCCNTDKCN	NMR	3.6	318K		Otting *et. al.* (10)*
	Tγ	LKC NQLIPPF	WKTCPKGKNL	CYKMTMRAAP	MVPVKRGCID	VCPKSSLLIK	YMCCNTDKCN	X-ray (1.55Å)	4.5	298K[§]	1TGX	Bilwes *et. al.* (*11*)
								NMR	3.5	318K	1CXO	Gilquin *et. al* (*12*).
	M4[†]	LKC NRLIPPF	WKTCPEGKNL	CYKMTMRLAP	KVPVKRGCID	VCPKSSLLIK	YMCCNTNKCN					
II	A1	LKC NKLIPIA	SKTCPAGKNL	CYKMFMMSDL	TIPVKRGCID	VCPKNSLLVK	YVCCNTDRCN	NMR	5.6	300K	2CDX	Jahnke *et. al.* (*13*).
	A2	LKC NKLVPLF	YKTCPAGKNL	CYKMFMVSNL	TVPVKRGCID	VCPKNSALVK	YVCCNTDRCN	NMR	3.0	293K	1CRF	Bhaskaran *et. al.* (*14*)
	A4	RKC NKLVPLF	YKTCPAGKNL	CYKMFMVSNL	TVPVKRGCID	VCPKNSALVK	YVCCNTDRCN	NMR	3.0	293K	1KBT	Jang *et. al* (*15*).
	A4b	LKC NKLVPLF	YKTCPAGKNL	CYKMFMVSNK	MVPVKRGCID	VCPKSSLLVK	YVCCNTDRCN	NMR	3.13	298K	1CHV	Jayaraman *et. al.* (*16*)
	M3	LKC NKLIPIA	YKTCPEGKNL	CYKMMLASKK	MVPVKRGCIN	VCPKNSALVK	YVCCSTDRCN	X-ray (2.5Å)	7.2	277K	1CDT	Rees *et. al* (*17*).
	O2	LKC KKLVPLF	SKTCPAGKNL	CYKMFMVAAP	HVPVKRGCID	VCPKSSLLVK	YVCCNTDKCN	NMR	5.0	300K	1CB9	Dementieva *et.al.* (*18*)
	A3	LKC NKLVPLF	YKTCPAGKNL	CYKMFMVATP	KVPVKRGCID	VCPKSSLLVK	YVCCNTDRCN	X-ray (1.9Å)	4.6	110K[§]	1H0J	Forouhar *et. Al.* (*3*)
								NMR	6.0	300K	1I02	Sue *et. al* (*19*).
	A5	LKCHNTQLPFI	YKTCPEGKNL	CFKATLKKFPLKFPVKRGCAD		NCPKNSALLK	YVCCSTDKCN	X-ray (2.19Å)	8.5	298K[§]	1KXI	Sun *et. al.* (*20*)
								NMR	3.7	318K	1CVO	Singhal *et. al.* (*21*)

* The NMR structures of CTX A6, M2, and M3 have not been determined yet; the information we used was the chemical shift assignments determined by O'Connell et al. (*9*) and this work. [§] The temperature of the X-ray is the data collection temperature. [†] The structure of CTX M4 has not been determined yet.

similarity with cyclolinopeptide A (CLA) and its analogues (*25*, *26*); these compounds mediate its immunosuppressive activity through a cyclophilin-dependent calcineurin inactivation (*27*).

EXPERIMENTAL PROCEDURES

Materials. CTXs were purified by applying crude venoms (*Naja atra* purchased from Snake Education Farm, Tainan, Taiwan; *Naja mossambica* and *Naja nigricollis* from Sigma Chemical, St. Louis, MO) to a SP-Sephadex C-25 ion-exchange column chromatograph (Amersham Pharmacia Biotech Limited) followed by HPLC on a reverse-phase C-18 (10 mm) column (NACALAI COSMOSIL AR-300) as described previously (*6*). The purity of all toxins was verified by SDS−PAGE, MS, and HPLC. The concentrations of CTXs were estimated from their absorbance maxima at 274 nm (molar extinction coefficients, $\epsilon^{274} = 3293.4$ cm^2 mol^{-1} for CTX A1, 3298.8 cm^2 mol^{-1} for CTX M5, 4692.8 cm^2 mol^{-1} for CTX A2−A4, A4b, and A6, 8629 cm^2 mol^{-1} for CTX M1, M2, and Tγ, 4682 cm^2 mol^{-1} for CTX M3, 4687.4 cm^2 mol^{-1} for CTX M4, and 3309.6 cm^2 mol^{-1} for CTX A5) (*28*). Dioleoylphosphatidylserine (DOPS, Avanti Polar Lipids, Birmingham, AL) was used without further purification. All other chemical reagents were obtained from Sigma or Merck.

HPLC−MS. The crude venoms of Taiwan cobra were injected into a LC−MS system directly after eliminating the insoluble part by centrifugation. The HPLC column that was used was the same as that mentioned above; at the end of the column, the effluent was divided into two flow paths: one was injected into a mass spectrometer (MICROMASS QUATTRO LC TANDER, Micromass UK Ltd.) and the other passed through a UV detector monitoring the effluent at 215 nm (Agilent 1100, Agilent Ltd.).

Circular Dichroism. CD spectra were recorded on an AVIV circular dichroism spectrometer (model 62ADS), interfaced with a computer. All CD spectra were measured with CTX (20 μM) in silica cells (path length of 1.0 mm). The spectra were measured at least five times on newly prepared samples, and results were averaged; baseline correction was carried out for each sample. The CD signal is reported as molar ellipticity [θ], calculated from the relationship $[\theta] = \theta_{abs}/(lc)$ in which θ_{abs} is the observed ellipticity (millidegrees), c is the concentration (molarity), and l is the length of the optical path (centimeters).

Vesicle Preparation. DOPS were dissolved in 10 mM Tris-HCl (pH 7.4). Small unilamellar vesicles (SUV) were prepared through ultrasonic irradiation of the lipid suspension for 10 min. Large vesicles were removed through ultracentrifugation (Beckman model LE-80, with a type 75TI rotor) of the sample (60 000 rpm for 1 h). The final SUV concentration was determined through a phosphate assay of the lipid headgroup phosphate (*29*).

CD Spectroscopy with Lipid Titration. The SUV stock solution was prepared at a high concentration (5 mM) to eliminate a dilution factor. The titration molar ratio (R_i) equals [lipid]/[protein]. Each CD spectrum was normalized according to an individual dilution factor.

Crystallization and Diffraction Data Collection. We achieved protein crystallization by the hanging-drop vapor-diffusion method at 291 K using screen kits (Hampton Research Crystal Screens) (*30*). Small crystals were obtained from one condition using sodium formate as a precipitant within 5 days of the initial screening. This condition was further refined to produce larger CTX A6 crystals using 2 μL hanging drops containing equal volumes of protein solution (10.0 mg/mL) and a reservoir solution containing sodium formate (2.2 M) and MES buffer (50 mM) at pH 6.0. The crystals that reached a terminal size of 0.3 mm × 0.25 mm × 0.06 mm in 2 weeks were used for experimental data collection.

The protein crystals were initially screened and characterized at protein crystallographic beamline BL17B2 equipped with an imaging plate detector (Raxis-IV++, Rigaku/MSC) at Taiwan's synchrotron (NSRRC). Data collection was completed at PX beamline BL12B2 equipped with a CCD

Table 2: Crystal Diffraction and Structural Statistics of CTX A6[a]

crystal data	
wavelength (Å)	1.00 (SPring-8, BL12B2)
temperature (K)	110
resolution range (Å)	25−1.6
space group	*R*32
no. of unique reflections	6187
completeness (%) (outermost shell)	95.6 (81.6)
I/σ_I (outermost shell)	15.1 (3.5)
average redundancy	11.5
R_{sym}[b] (%)	7.2 (24.6)
mosaicity	0.601
unit cell parameters	$a = 39.62$ Å, $b = 39.62$ Å, $c = 153.57$ Å, $\gamma = 120°$
no. of molecules per asymmetric unit	1
refinement results	
initial model (%) (25−1.6 Å)	R[c] $= 33.5$, $R_{free} = 34.1$
model after refinement (%) (25−1.6 Å)	R[c] $= 23.9$, $R_{free} = 28.0$
rmsd for bond lengths (Å)	0.005
rmsd for bond angles (deg)	1.424
total no. of amino acid residues	60
total no. of protein atoms (non-hydrogen)	461
total no. of water molecules	36

[a] Reflections of a $2\sigma_I$ cutoff were applied in generating the statistics. [b] $R_{sym} = \sum_h\sum_i[|I_i(h) - \langle I(h)\rangle|/\sum_h\sum_i I_i(h)]$, where I_i is the ith measurement and $\langle I(h)\rangle$ is the weighted mean of all measurements of $I(h)$. [c] $R = \sum_h|F_o - F_c|/\sum_h F_o$, where F_o and F_c are the observed and calculated structure factor amplitudes of reflection h, respectively.

detector (Quantum-4R, ADSC) using synchrotron radiation as a source of X-rays with a wavelength of 1.0 Å at SPring-8 in Japan. The crystal was transferred into a cryoprotectant solution containing glycerol (15%) and mounted on a glass loop (0.2−0.3 mm, Hampton Research Co.). A 180° data set (1° oscillation frame, each exposed for 40 s) to 1.6 Å resolution was collected using a distance from the crystal to detector of 120 mm at 110 K. The data were indexed, integrated, and scaled using *HKL2000* (*31*). Analysis of the diffraction pattern indicates that crystals belong to space group *R*32 with the following unit cell dimensions: $a = 39.62$ Å, $b = 39.62$ Å, $c = 153.57$ Å, and $\gamma = 120°$. The data set is 95.6% complete with an internal agreement (R_{sym}) of 7.2%. Assuming one molecule per asymmetric unit, the Matthew's coefficient is estimated to be 1.74 Å^3 Da^{-1}, which corresponds to a solvent content of 29.1% (*32*). The low solvent content explains the good quality of crystal diffraction beyond 1.6 Å resolution. Details of data statistics are given in Table 2.

Crystal Structure Determination and Refinement. The method of solution of the crystal structure of CTXA6 was molecular replacement (*33*) using the *Toxin γ* (*N. nigricollis*) monomer structure (PDB entry 1TGX), of which nonconserved residues were altered to alanines as a search model, using CNS version 1.1 (*34*). The rotation and translation function searches were calculated using data in the range of 15−3.5 Å resolution and a Patterson radius of 25 Å, and gave a unique solution with a large correlation between observed amplitudes for the crystal and calculated amplitudes for the model.

Further crystallographic refinement was carried out using CNS version 1.1. Throughout the refinement, a random selection (10%) of the data was set aside as a "free data set", and the model was refined against the data with $F \geq 2\sigma_I$ (working data set) (*35*). The protein model obtained through molecular replacement was initially refined using the data from 25.0 to 1.6 Å resolution. The individual *B* values were first restrained to 20.0 Å^2 and were refined only in the last cycles of refinement. After rigid-body refinement, the solution was refined to an initial *R*-factor of 0.335 and R_{free} of 0.341 in the resolution range of 25−1.6 Å. This refinement was followed by simulated annealing with a slow cooling protocol provided in CNS, applied to data between 25.0 and 1.6 Å. A starting temperature of 2500 K was gradually decreased to 300 K in 25 K steps using a time step of 0.5 fs between energy calculations. For this resolution range, the *R*-factor was decreased to 0.318 and R_{free} to 0.324. Throughout the refinement, the composite omit maps with $2F_o - F_c$ coefficients were calculated with CNS and visualized using O version 7.0 (*36*), and the model was built and adjusted iteratively as required. In later stages of the refinement, a bulk solvent correction was applied and individual *B*-factors were adjusted with an *R*-factor of 0.265 and an R_{free} of 0.291. The PICKWATER subroutine from CNS served to define peaks in difference maps (3σ cutoff level), to locate water molecules; a water molecule was accepted if the identified peak correlated with a separate peak in the corresponding $2F_o - F_c$ electron density map, and if one or more hydrogen bonds (3.3−2.3 Å) were identifiable. On the basis of this criterion, 36 water molecules were located. The protein model and water molecules were then subjected to another run of positional, simulated annealing and individual *B*-factor refinement.

The final model of CTXA6 contains 461 non-hydrogen protein atoms and 36 solvent molecules (PDB entry 1UG4). For data between 25.0 and 1.6 Å resolution, the resulting model had a final *R*-factor of 23.9% and an R_{free} of 28.1% (Table 2). The correctness of stereochemistry of the model was verified using PROCHECK (*37*), calculations of rms deviations from ideal values for bonds, angles, dihedral angles, and improper angles performed in CNS. For all criteria used by PROCHECK, the model was flagged as being better than or within good regions. The calculations also showed satisfactory stereochemistry with rms deviations from ideality (*38*) in bond lengths of 0.005 Å and angles of 1.424°. In a Ramachandran plot (*39*), 98.0% of residue dihedral angles are in the most favored and additionally allowed regions, and no main chain dihedral angle is observed in disallowed regions.

NMR Spectroscopy. CTX A6 was dissolved in a 90% H_2O/10% D_2O mixture or 100% D_2O to a final concentration of 2 mM for two-dimensional ^{1}H TOCSY, NOESY, and ROESY NMR experiments. For the ^{13}C−^{1}H HSQC NMR experiment, CTX A6 (4 mM in 100% D_2O) was used to improve the signal-to-noise ratio. The pH of the sample was controlled at 3.6 ± 0.01 with NaOD and DCl. We performed an NMR study at this specific pH because the previous NMR study of other group I CTX homologues, i.e., Tγ and CTX M1, was performed at pH 3.5−3.6, and Tγ and CTX M1 were suggested to adopt an all-*trans*-Pro conformation at the loop I region. In contrast, the X-ray structure of Tγ determined at pH 4.5 was shown to adopt a *cis*-Pro peptide conformation between two proline residues of PPxY near the region. A comparison of the NMR structure of CTX A6 determined at pH 3.6 with its X-ray structure determined at pH 6.0 could then help us resolve the discrepancy of structural differences in Tγ between the solution and crystal state. With the exception of the residue at position 11 (Tyr vs Trp), the amino acid sequences of CTX A6 and Tγ are

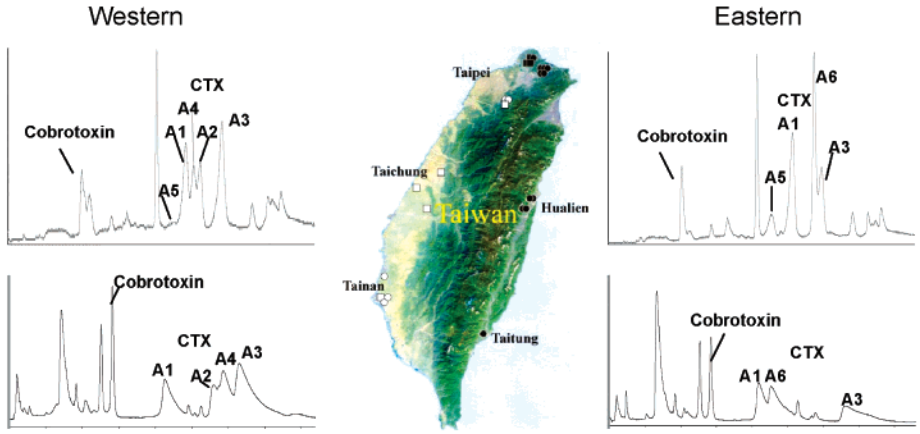

FIGURE 1: Comparisons of CTX homologues identified in Taiwan cobra venom of eastern and western origin. C18 reverse-phase (top panels) and Mono-S cation-exchange (bottom panels) HPLC chromatography of *N. atra* venoms collected from cobra caught in the wild exhibit distinct CTX compositions.

essentially the same. There was no indication of protein aggregation or degradation as judged from the quality of ^{1}H NMR spectra during the experiments (up to 318 K for 1 week) and the period of sample storage (several months at 253 K). The pH measurement of the sample after acquisition of spectra showed the pH variation to be smaller than 0.1. The pH of samples containing 100% D_2O was corrected according to the isotopic effect as pD = pH* + 0.4.

All NMR experiments were carried out on a BRUKER Advance 500 spectrometer equipped with a 5 mm triple-resonance probe. Two-dimensional ^{1}H COSY, DQF-COSY, TOCSY (mixing period τ_m = 90 ms), NOESY (τ_m = 60, 100, and 200 ms), and ROESY (τ_m = 90 ms) spectra were obtained at 318 K as described previously. Either a pulsed-field gradient with the 3-9-19 WATERGATE sequence or presaturation was used to suppress the water signal. ^{1}H chemical shifts were referenced to 2,2-dimethyl-2-silapentane-1-sulfonate (DSS) at 0.015 ppm, and ^{13}C chemical shifts were indirectly referenced according to a consensus *E* ratio (^{13}C/^{1}H) of 0.251 449 530. Spectra were typically acquired with 2048 complex data points in the t_2 dimension and 512 points in the t_1 dimension with a time-proportional phase increment (TPPI) method. Data processing was performed on a workstation (Silicon Graphics O2) with XWINNMR.

^{1}H NMR spectra were assigned using standard methods (*40*, *41*). The scalar-coupled spin systems were first identified in TOCSY and DQF-COSY spectra; the sequential connectivity was then determined using NOESY and ROESY experiments. The NOESY spectra with a τ_m of 100 ms (Tγ paper) were used for NOE distance estimation because some NOEs were too weak to be correctly evaluated in terms of distance when using NOESY spectra with a τ_m of 60 ms (*10*). The relationship between NOE intensity and τ_m was still linear under 100 ms; we also used ROESY with a mixing period of 90 ms to eliminate the possibility of spin diffusion (*42*). A natural abundance ^{1}H−^{13}C HSQC spectrum was recorded to resolve the C_β and C_γ resonances of prolines.

Signals present for both NOESY (τ_m = 100 ms) and ROESY (τ_m = 90 ms) spectra were recognized as real structural constraints. A $1/r^6$ dependence was used for NOE. When the NOE was applied to degenerate protons, a range was given to account for the possibility that these degenerate protons would contribute equally or disparately to the observed NOE. Reference to a distance of 1.75 Å between two methylene protons enabled distance calibration.

Molecular Modeling. The modeling of the WW domain−CTX A6 complex for both group I and II was performed on the basis of the structure of a WW domain-containing fragment of dystrophin in complex with β-dystroglycan (*43*). The complex structure (PDB entry 1EG4) provided a 1.9 Å high-resolution view of the WW domain with the PPxY peptide (where x represents any amino acid). The PPxY binding motif of β-dystroglycan was replaced with CTX A6 loop I residues ($P_8P_9F_{10}Y_{11}$), and the potential energy was minimized with the cvff force field in the "Discover" module of Insight II. The structure of group II of CTX A6 with a trans conformation between two proline residues of loop I was adapted from the NMR structure of CTX M1 with a substituted residue (Tyr 11 for Trp).

The SH3 domain−CTX A6 complex was modeled on the basis of the solution structure of *c-Src* SH3 in complex with a class II peptide of AFAPPLPRR by multidimensional NMR spectroscopy (*44*). It showed a typical complex structure of the SH3 domain and class II peptide of PxxPx+ (PDB entry 1PRL). By swapping the SH3 binding motif coordinates with those of residues A29−K35 of CTX, we were able to generate a new structure of CTX A6 suitable for binding to *c-Src* SH3. Pro30, Pro33, and Arg36 of CTX A6 can be observed to interact with the aromatic rich and negatively charged areas without serious steric hindrance between CTX A6 and *c-Src* SH3.

RESULTS

CTX Purification and Distribution. Shown in Figure 1 are the representative elution profiles of cobra venoms collected at indicated geographic locations of Taiwan using either cationic exchange or a reverse-phase HPLC column. All the cobras were caught in the wild by a local office and kept at the Taipei Zoo. The amino acid sequences (Table 1) were confirmed by mass spectrometer analysis by matching with the available NCBI Entrez protein data bank and by the same elution position using the CTX stocks in the laboratory. Both analytical methods show the presence of group I CTX A6 for venoms of eastern origin, but there is no detectable CTX A6 for venoms of western origin. In contrast, the detected CTX fractions for venoms of western origin are all group II CTX, including CTX A1−A5, as identified from known

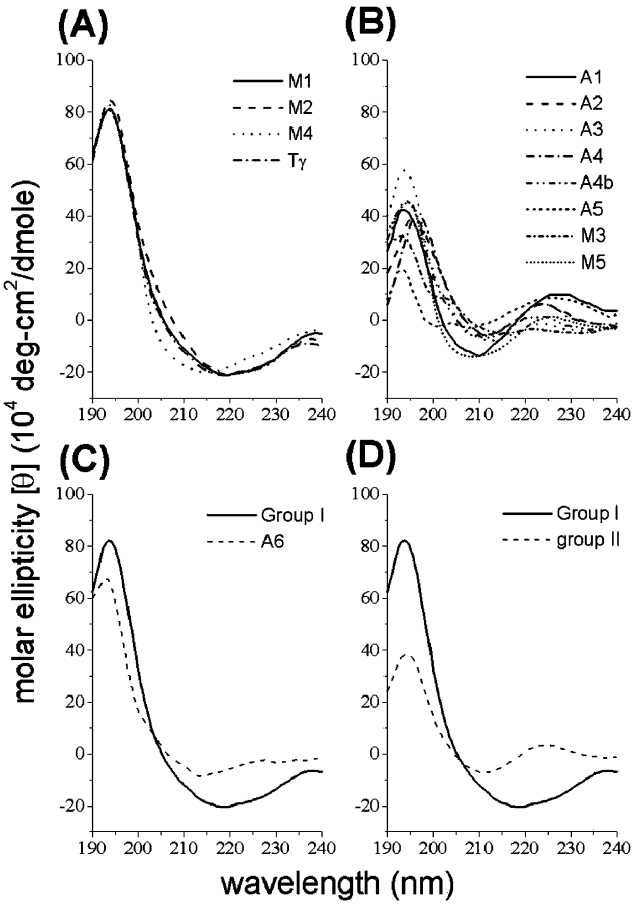

FIGURE 2: CD spectra of CTX isolated from *N. atra*, *N. mossambique*, and *N. nigricollis* venom: (A) group I CTX, (B) group II CTX, (C) averaged CD spectra of group I CTXs and CTX A6, and (D) averaged CD spectra of the two group CTXs. Classes are defined according to ref *8* and Table 1.

CTX standards and mass spectra. Other than CTX A2 and A4, other group II CTXs (A1, A3, and A5) can be observed in venoms of eastern origin. In general, the expression levels of CTX detected in venoms of eastern origin are conserved, with fractions of CTX A1, A3, A5, and A6 falling in a range of the detected CTX, 35, 25, 7, and 32% (±2%), respectively. For CTX identified in venoms of western origin, one can further classify the venoms into two subtypes according to the quantity of observed CTX homologues (data not shown). Apparently, the geographic location in a highly populated western area is not an important factor in forming the subgroup because both subgroups can be identified for venom samples collected in northern and southern Taiwan.

Circular Dichroism Analysis. We classify CTX A6 as a group I CTX not only because of its primary sequence of LIPPF at the loop I region being identical to that of other group I CTXs but also because of its characteristic secondary structure as detected in circular dichroism (CD) spectra. We obtained CD spectra from our own CTX stock and confirm a previous conclusion that CD spectra of group I CTXs have a more intense positive band at 192.5 nm, but lack a broad positive band near 225 nm for group II CTXs (Figure 2). Unlike those of most group I CTXs, the negative trough near 220 nm is significantly smaller for CTX A6. This condition is consistent with the observation that the amino acid residue at position 11 is Tyr, instead of Trp, for CTX A6. CD spectra

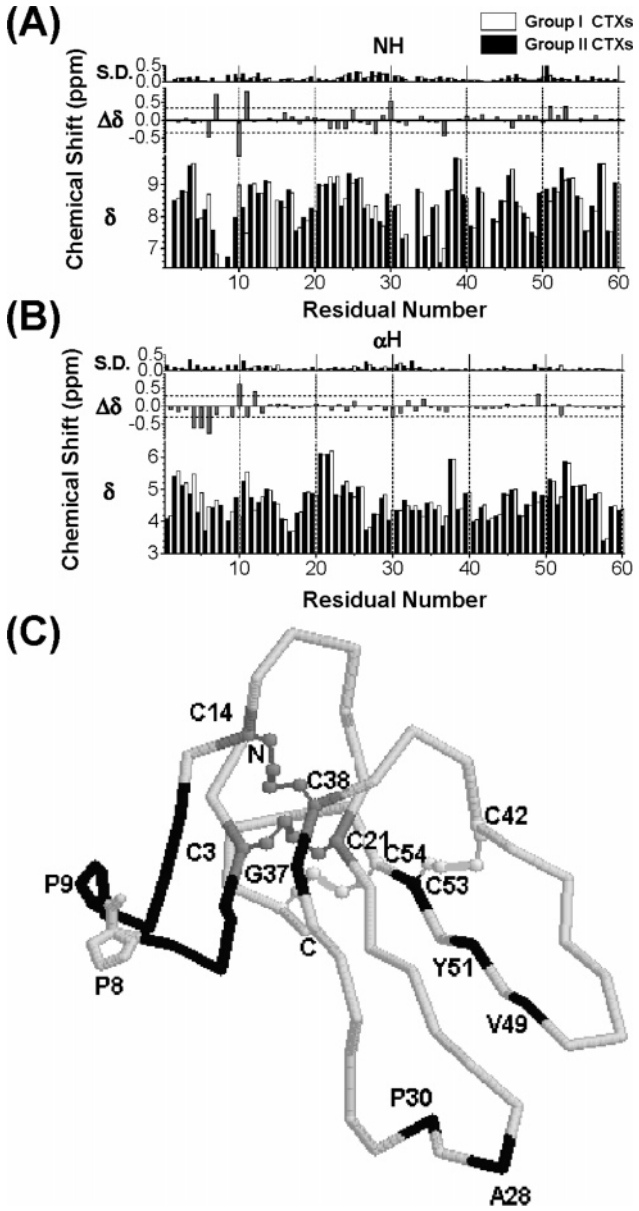

FIGURE 3: Comparison of chemical shift variation of NH (A) and αH (B) between group I and II CTXs as indicated by the standard deviation (top panel), the difference between group II and I CTXs (middle panel), and the averaged chemical shift of group I and II CTXs (bottom panel). The analyzed chemical shift data were all available, including those for CTX M1, M2, Tγ, and A6 of group I and CTX A1−A4, A4b, M3, and O2 of group II. (C) Hot spot of chemical shift variation sites, with CTX A6 taken as the model. Residues with a chemical shift variation of >0.35 ppm (for NH) or >0.29 ppm (for αH) are colored black; also shown are four disulfide linkages in CTX. The two disulfide bonds (C3−C21 and C14−C38) connected to loop I are colored dark gray and the other two light gray. P8 and P9 positions are depicted at the left side of the molecule.

of proteins containing Trp have been suggested to give a negative signal near 220 nm (*45*, *46*).

Despite the fact that group I and II CTXs are both three-fingered toxins with a similar extent of antiparallel β-sheet structure, it is intriguing to see that their representative CD spectra differ significantly. Previous analysis of the 225 nm CD band of elapid three-fingered toxin indicated that the intensity of this CD band is sensitive to conformational change associated with the disulfide bond (*8*, *47*). A much weaker positive band at 192.5 nm was interpreted as

Table 3: ^{1}H Chemical Shifts of CTX A6 at pH 3.6 and 318 K[a]

	$^3J_{NH-\alpha H}$	NH	αH	βH	γH	others
L1			4.176	1.827/1.601	1.520	δCH$_3$, 0.840/0.784
K2	10.2	8.524	5.473	1.540	1.484/1.433	δH; εH, 2.904; εNH$_2$
C3	9.85	8.583	5.159	2.975/2.614		
N4	8.79	9.719	5.467	2.694/2.259		γNH$_2$, 6.878/6.392
Q5	8.84	7.893	4.851	2.164	1.941	δNH$_2$
L6		8.684	4.429	1.817	1.603	δCH$_3$, 0.864/0.826
I7	9.14	6.813	4.665	1.895	1.341	δCH$_3$, 0.858
					CH$_3$, 0.981	
P8				1.594	2.005/1.853	δH, 3.719/3.585
P9			4.290	2.370/2.005	1.788/1.232	δH, 3.337/3.143
F10		8.841	4.136	3.480		3,4,5H, 7.345; 2,6H, 7.145
Y11	8.79	7.423	5.451	3.315/2.554		aromatic H, 6.846
K12		8.815	4.549	1.713	1.327/1.169	δH; εH, 3.038; εNH$_2$
T13	8.11	8.637	4.648	4.059	CH$_3$, 1.274	
C14	7.02	8.915	4.774	3.540/2.834		
A15	5.87	8.506	4.290	CH$_3$, 1.455		
A16	6.03	8.204	4.103	CH$_3$, 1.379		
G17	9.75	8.617	4.255/3.666			
K18	8.87	7.708	4.243	2.117	1.366/1.115	δH, 1.591/1.414; εH, 2.956
N19	8.79	7.740	4.906	2.999/2.658		γNH$_2$, 7.377/6.846
L20	8.77	8.190	4.816	1.643	1.520	δCH$_3$, 0.863/0.747
C21	8.88	8.934	6.072	3.068/2.994		
Y22	9.32	9.187	6.121	3.138/3.009		2,6H, 6.720; 3,5H, 6.628
K23	8.79	9.099	4.799	1.836/1.731	1.495/1.425	δH, 1.684; εH, 2.915; εNH$_2$
M24	8.82	8.248	5.261	1.428	1.758/1.647	εCH$_3$
F25	9.33	8.962	4.975	2.912		4H, 7.209; 3,5H, 7.082; 2,6H, 6.873
M26	8.92	9.406	5.070	2.312/2.002	2.800/2.623	εCH$_3$
V27	5.83	8.168	3.613	1.999	0.984/0.941	
A28	6.03	8.171	4.247	CH$_3$, 1.420		
A29	8.84	7.690	4.875	CH$_3$, 1.289		
P30			4.266	1.782/1.729		3.596
K31	7.38	8.101	4.113	1.929/1.767	1.382/1.295	δH, 1.612; εH, 2.940; εNH$_2$
V32		7.465	4.552	2.150	0.903	
P33			4.409	1.696	2.063/1.836	δH, 3.930/3.820
V34	8.80	8.758	4.172	2.048	1.011	
K35		7.346	4.561	2.057	1.677/1.555	δH, 1.906/1.821; εH, 3.057; εNH$_2$
R36	8.76	8.228	4.477	1.690/1.486	1.326	δH, 2.806/2.682; NH, 8.347
G37		6.934	4.277/4.159			
C38	8.78	8.656	5.919	3.561/2.905		
I39	5.94	9.748	4.406	1.684	1.606/1.379	δCH$_3$, 0.361
					CH$_3$, 0.511	
D40	8.73	8.506	4.886	2.809		
V41	9.27	7.573	4.043	1.744	0.748	
C42		8.705	4.499	3.071/2.763		
P43			4.054	1.698/0.195	1.245/0.704	δH, 3.937/2.542
K44	8.63	7.793	4.193	1.811	1.716/1.554	δH; εH, 3.037; εNH$_2$
S45	6.42	8.422	4.785	4.432/4.044		
S46	9.99	9.338	4.975	4.431/3.977		
L47	6.04	8.154	4.198	1.744	1.628	δCH$_3$, 0.958/0.926
L48		7.966	4.533	1.721	1.650	δCH$_3$, 0.947/0.878
V49	9.98	7.404	4.716	1.885	0.864/0.734	
K50	9.99	8.583	4.728	1.661	1.316/1.085	δH; εH, 2.839; εNH$_2$
Y51	8.95	8.189	5.287	2.795/2.650		2,6H, 6.777; 3,5H, 6.615
V52	8.83	8.864	4.523	2.038	1.126/1.047	
C53	10.31	9.215	5.821	3.808/3.044		
C54	6.73	9.203	5.092	3.637/3.449		
N55	8.88	8.547	5.132	3.355/2.659		γNH$_2$, 6.674/7.432
T56	8.74	7.532	4.697	4.292	CH$_3$, 1.211	
D57		8.127	4.839	2.565/2.394		
R58	5.88	9.634	3.457	2.217/1.783	1.490/0.986	δH, 2.894/2.630; NH
C59	7.32	7.545	4.469	3.634/3.377		
N60	8.77	9.006	4.390	2.741/2.306		γNH$_2$, 7.766/7.570

[a] Values were calibrated with respect to 2,2-dimethyl-2-silapentane-5-sulfonate (DSS) at 0.0 ppm.

indicating a different degree of β-sheet twisting. As there are four disulfide bonds located near the core of the three-fingered CTX toxin to tighten the large triple-stranded, antiparallel β-sheet and short double-stranded β-sheet (see, for instance, Figure 3), significant modification of the dihedral angle in the disulfide bond would result in a structural alteration of the β-sheet twisting. Therefore, the two aforementioned interpretations on the observed CD spectra for the two groups of CTX molecules are not mutually exclusive. On the basis of available extensive data for the proton NMR chemical shifts for both group I and II CTXs (Table 1; see also Table 3), it would be interesting to examine whether such an interpretation might be supported through NMR data.

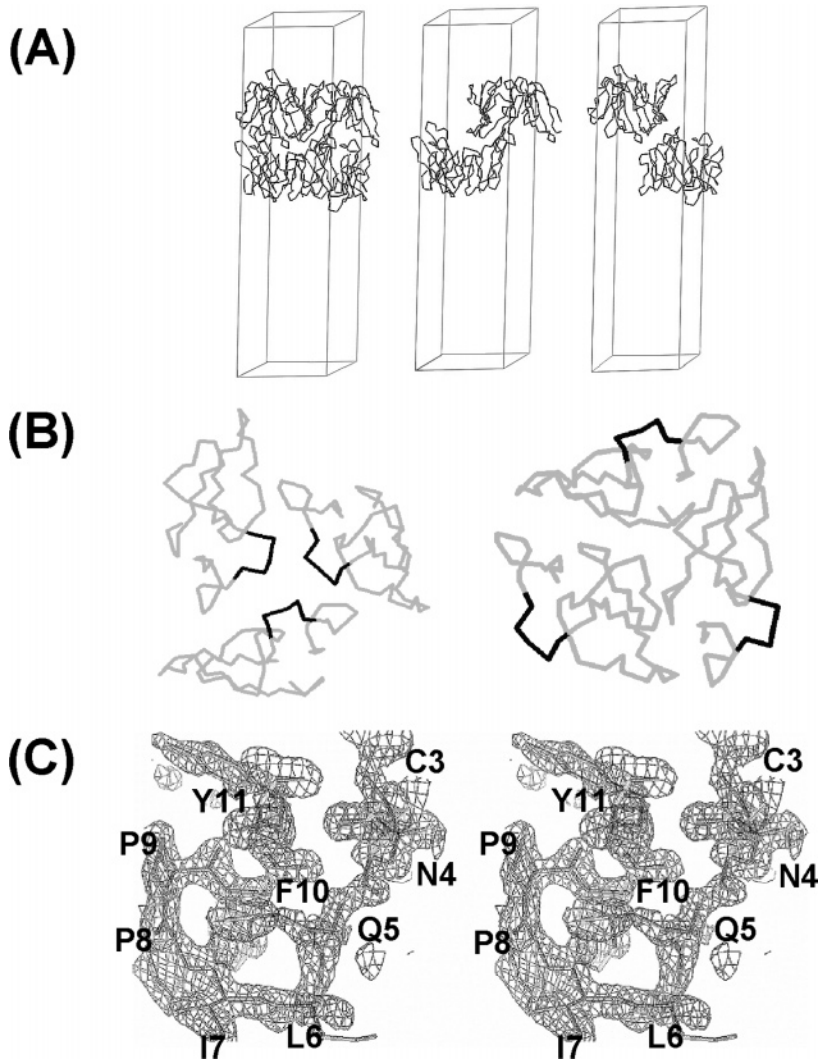

FIGURE 4: X-ray structure of CTX A6. (A) Crystal packing of CTX A6. At the left is the packing between two layers of five CTX A6 monomers. The packing between two layers of three CTX A6 monomers is shown in the middle and right panels to illustrate packing of the two types: one is core region inward (middle) and the other core region outward (right). (B) Top view of packing of these two types: core region inward (left) and core region outward (right). The dark lines indicate the β-turn composed of A15−K18 just on top of the core region. (C) Stereoview of the $|2F_o - F_c|$ electron density map of the loop I region (residues 4−10 were omitted while the map was calculated).

NMR Chemical Shift Analysis. Figure 3 shows a statistical analysis of the chemical shift differences between group I and II CTX for both NH and αH of the CTX polypeptide main chain. As illustrated in the schematic CTX structure diagram, the most significant difference in chemical shift between the two homologous groups is located at loop I (amino acids 3−12) and the antiparallel β-sheet (amino acid positions 49, 51, and 53) regions. The chemical shift difference observed in the loop I region is easily understood since the overall conformations of loop I between group I and II CTXs are indeed different as we will demonstrate by using the X-ray and NMR method in the following sections. Other chemical shift differences observed within the antiparallel β-sheet region are more intriguing. Since Cys3−Cys21 and Cys14−Cys38 disulfide bonds connect the two regions, we suggest that their difference might be an indirect effect of the conformational difference in the loop I region between the two CTX groups. More specifically, we propose that the twisting of the antiparallel β-sheet, as reflected by the observed difference in both CD and NMR spectra, is significantly perturbed due to the conformational change in disulfide bonds connecting the two regions. In fact, the two designated disulfide bonds are located near the hydrophobic core centered at Gly37 and Tyr22. It suggests that a delicate difference in the hydrophobic packing near the region might exist between group I and II CTXs. The interpretation also provides a possible explanation for the chemical shift difference detected at Gly37. The difference is likely also significant as the standard deviation of the analyzed chemical shift difference is smaller than those detected near the tip of loop II. Taken together, the available data are consistent with a model to suggest that the loop I conformational difference between group I and II CTXs plays a dominant role in triggering an overall conformational change at both the hydrophobic core and the antiparallel β-sheet region as detected by both CD and NMR chemical shift analysis.

X-ray Crystal Structure of CTX A6. To obtain more detailed information about the exact conformational difference between CTXs of the two groups, we grew a CTX A6 crystal and determined its structure at 1.6 Å resolution. As shown in Figure 4, the crystal packing of CTX A6 molecules exhibits a trimeric structure similar to that of other group I

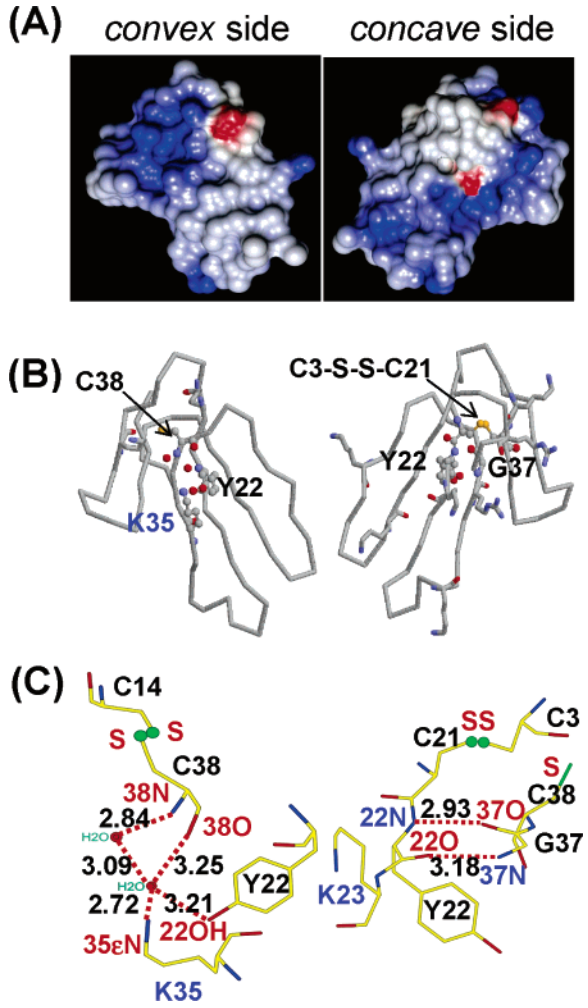

FIGURE 5: Convex side and concave side of CTX A6. (A) Surface of electrostatic potential of CTX A6. (B) Convex side and concave side views of the CTX A6 backbone, in which all positively charged residues are shown as stick models; also shown are C38 and Y22 on the convex side and G37, Y22, and C3 on the concave side. (C) Enlarged view of the core region. Also shown are two water molecules supposed to form a water network with the core region of the CTX A6 convex side, with distances between related atoms in angstroms.

CTXs of toxin γ (*11*). Two potential glycosaminoglycan binding pockets located at the respective convex and concave sides of the slightly curved CTX molecule, as illustrated in Figure 5, emphasize the importance of the charge distribution of CTX homologues in modulating CTX function. Upon inspection of the hydrophobic core located near Gly37 at the concave side, one can see that both the carbonyl and NH groups of Gly37 form hydrogen bonds with the main chain of Tyr22. As the neighboring residue of Cys21 is covalently connected to Cys3 near the N-terminal end of loop I through the disulfide bond, any significant conformational alteration occurring in the loop I region also affects the hydrophobic packing near Gly37. When the molecule is flipped to the convex side, there is an anionic binding pocket with an extensive water network to connect the side chain of Tyr22, Lys35, and the main chain of Cys38. Again, Cys38 is connected to Cys14 at the other end of loop I through a disulfide bond. As anionic ligands such as heparan sulfate or nucleotide triphosphate are known to interact with CTX at the aforementioned anionic binding pocket (*48*, *49*), it appears that CTX molecules are interconnected through loop I in a delicate manner with the hydrophobic core and anionic binding pocket.

Structural Comparison between the Solution and Crystal State. The loop I conformation of CTX A6 adopts a type VIa turn (*50*) with a cis peptide bond between the two prolines of the conserved LIPPF sequence. Such a conformation of the banana-twisted type is reported for the crystal structure of other group I CTXs of toxin γ. As the amino acid sequences of all available group I CTXs are conserved in the loop I region, it is surprising to find that the NMR solution structures for toxin γ and CTX M1 were previously reported to adopt a more extended loop I conformation with a trans peptide bond between the two proline amino acid residues. Such a discrepancy does not exist for other CTX molecules, such as group II CTX A3 and A5, with the X-ray and NMR structures both known (Figure 6). Previous studies of the structure−function relationship on the cytotoxicity of CTX by chemical modification indicate that the amino acid residues located in loop I play a crucial role in the action of CTX toward many cells, including cardiomyocytes (*1*, *51*, *52*). It is therefore important to establish whether the crystal and solution structures of group I CTXs such as toxin γ or CTX A6 are distinct.

First, we examine the molecular packing of CTX A6 in the crystal to determine whether there is direct interaction between CTX molecules in the loop I region. As shown in panels A and B of Figure 4, two orientations of trimeric CTX with either an inward or outward tight turn formed by the amino acid residues from Ala15 to Lys18 can be seen as alternatively stacking into two layers. The three-fingered loops of the CTX trimer with an inward tight turn are packing against each other. Further scrutiny of the molecular interaction reveals a hydrophobic interaction involving mainly the loop II region. The loop I region is surrounded by water molecules of hydration to a significant extent. There is no evidence that the loop I conformations of group I CTX A6 and toxin γ determined by X-ray diffraction are dominated by the crystal packing.

Second, we test whether NMR data obtained for a solution state might be misinterpreted as an unambiguous interpretation of NMR data for the proline−peptide bond to adopt a cis or trans conformation based simply on ^{1}H NMR spectra is known to be difficult. Recent advances in multinuclei NMR spectroscopy have shown that the ^{13}C NMR chemical shift can assist in resolving this difficulty because a chemical shift plot of $^{13}C_\beta$ versus $^{13}C_\gamma$ resonance reveals that trans and cis Xaa−Pro bonds are located in distinct regions divided by the diagonal line of the plot (*53*). As shown in Figure 7, Pro9 in both CTX A6 and toxin γ molecule is the only amino acid residue showing a distinct ^{13}C NMR chemical shift that can be classified as a cis peptide bond conformation.

With the known loop I conformation determined through X-ray diffraction, we inspect whether the detectable ^{1}H NMR NOE can be consistently interpreted to adopt a type VIa turn for loop I in the solution state. As shown in Figure 8, the banana-twisted conformation, but not the more extended loop, predicts detectable NOEs for the side chain protons of Phe10 with Ile7 αH and Leu6 αH, respectively. The presence of a detectable NOE cross-peak between Pro8 βH and Pro9 αH is also consistent with this interpretation. Unfortunately, as in previous work on Tγ and CTX M1 (*9*, *12*), we could

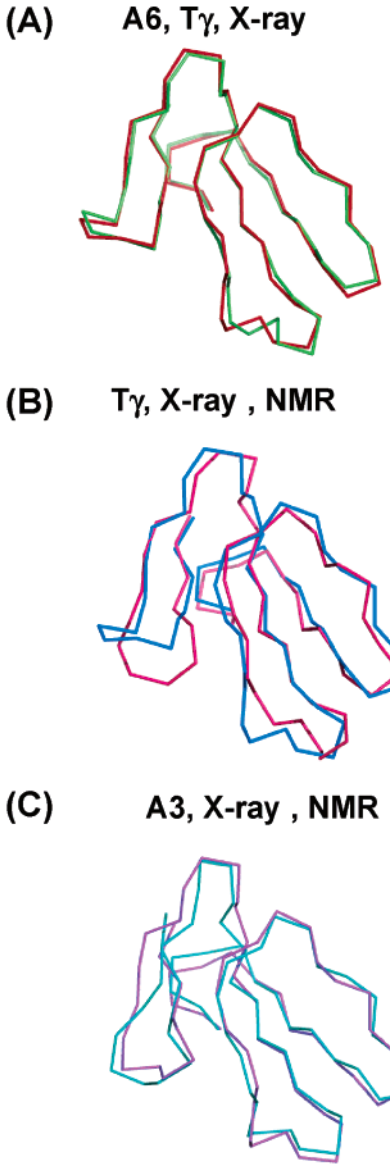

FIGURE 6: Convex side view and loop I conformation of CTX. (A) Superposition comparison between the X-ray three-dimensional structures of CTX A6 (green) and Tγ (red). (B) Superposition comparison between X-ray (blue) and NMR (pink) structures of class I CTX Tγ. (C) Superposition comparison between X-ray (magenta) and NMR (cyan) structures of class II CTX A3. The most significant difference is at loop I, namely, the cis and trans conformations of the P8−P9 peptide bond of class I and II CTXs.

not observe Pro8 βH in CTX A6; therefore, the NOE criteria for the cis peptide conformation are not available. Finally, we identify a detectable NOE between Gln5 γH and Tyr11 αH. With the type VIa turn conformation, it would imply that the side chain of Gln5 also forms a hydrogen bond with the carbonyl group of Ile7 to stabilize the turn in the solution state. We therefore conclude that the loop I conformation of group I CTXs adopts a type VIa turn in both crystalline and solution states.

We emphasize that the structural discrepancy of Tγ at the loop I region between the solution and crystalline state is not due to the different pH condition, i.e., pH 3.5 and 4.5, respectively, used in those studies. First, there are no titratable amino acid residues within the studied pH range near the loop I region of Tγ. Second, we could observe consistent NMR and X-ray structure of CTX A6 despite their different

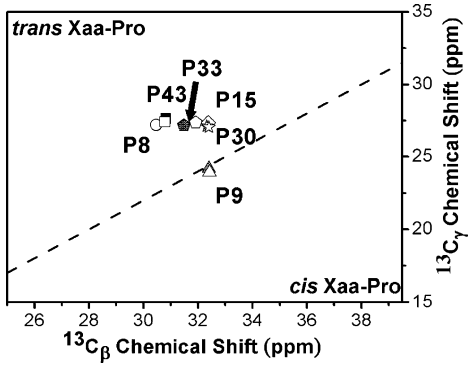

FIGURE 7: Plot of $^{13}C_\beta$ vs $^{13}C_\gamma$ of all prolines in CTX A6 and Tγ. The dashed line is a criterion ($\Delta^{13}C_\beta - {}^{13}C_\gamma \geq 8$ ppm) for identifying the cis conformation of proline. Filled and empty symbols represent data for A6 and Tγ, respectively. The symbols are defined as follows: circles for P8, triangles for P9, diamonds for P15, stars for P30, pentagons for P33, and squares for P43.

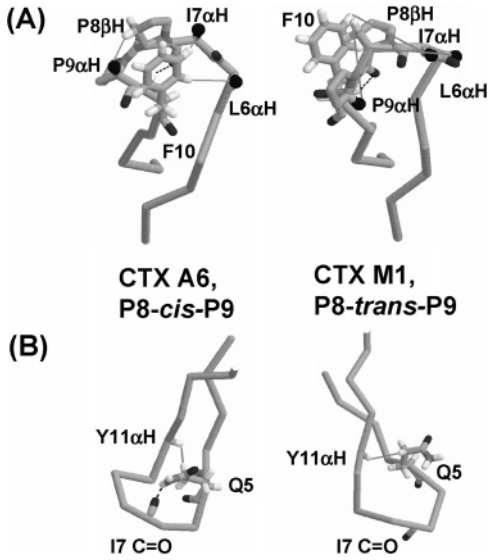

FIGURE 8: Cis and trans conformations of loop I of CTX. We take CTX A6 and CTX M1 conformations as examples of cis and trans conformations of CTX, respectively. In panel A are views of the relative position of the side chain of Q5: in the cis conformation, the terminal NH group of the side chain of Q5 can form a H-bond with the backbone, but this H-bond cannot be formed in the trans conformation of CTX. Also shown are those most significant distance variations listed in Table 2: P9 αH−P8 βH, I7 αH−F10 ϵH, and L6 αH−F10 δH distances are connected by solid gray lines, and the hydrogen bond related to F10 NH is plotted as a dashed line (F10 NH−I7 O in A6 and F10 NH−P8 O in M1). In panel B, the inverted loop I conformation is shown to illustrate the difference in the loop I conformation: the peptide bond between P8 and P9 is cis in A6 but trans in M1.

experimental pH conditions, i.e., pH 3.6 and 6.0, respectively. In fact, we also performed a similar NMR study of both CTX A6 and Tγ at pH 6.0, showing the same loop I conformation based on chemical shift analysis (data not shown).

Lipid-Induced Conformational Change. After establishing that the preferred loop I conformations of group I and II CTXs are different and adopt a banana-twisted and extended-loop shape, respectively, we address the question of their potential biological significance. Both computer simulation and binding measurements indicate that the presence of a cis peptide bond in loop I makes it less favorable for its interaction with lipid bilayers (*18*, *54*). Using CD spectra, we show in Figure 9 that group I CTXs are transformed into

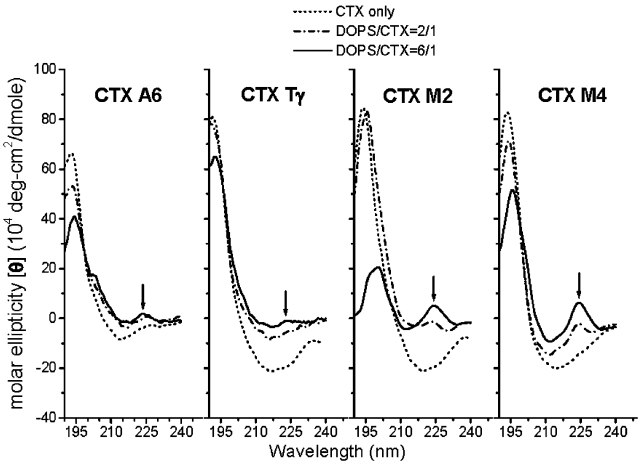

FIGURE 9: CD spectra of class I CTXs with varied ratios of DOPS. The dotted, dashed, and solid lines indicate the CD spectra of pure CTX, a 2/1 DOPS/CTX mixture, and a 6/1 DOPS/CTX mixture, respectively. The arrows indicate the appearance of a hump at ~225 nm.

a conformation similar to that of group II CTXs upon binding to negatively charged membranes of DOPS as indicated by the decreased intensity of the CD band at 192.5 nm and the increased intensity at 225 nm. Unfortunately, the binding of CTX to negatively charged vesicle also induces significant aggregation of the sample at high CTX concentrations. It is not possible to perform a NMR study to provide additional experimental data to support the conclusion at present. Nevertheless, the interpretation is consistent with the previous observation that the cis peptide bond in loop I is less likely to interact with the lipid bilayer. Potential protein targets of group I CTXs after cell internalization are therefore discussed on the basis of the structural similarity of the determined loop I conformation with other protein molecules.

DISCUSSION

Toxicity and Immunogenecity of Cobra Venoms from Different Geographic Locations. The major symptom of a victim of cobra snakebite, if not death from the action of neurotoxin or CTX, is severe tissue necrosis and inflammation of skin (*55*). The symptoms and lethal potency induced by venoms collected at separate geographic locations vary significantly (*55*). For instance, not only is the specific toxicity of cobra venoms collected from western Taiwan approximately twice as potent as that collected from eastern Taiwan, but one can also detect a significant difference in the neutralization titer of the antibody produced by venoms from the two regions. As diverse CTXs of up to approximately six or seven homologues are known to be present in cobra venom (*22*), it is of interest to see whether the expression levels of various CTXs differ for cobra venoms collected from separate geographic locations. Relative proportions of toxins in expressed venoms are suggested to vary significantly for snakes of the same species but from separate geographic locations (*56*). As group I CTX A6 can be observed in only eastern cobra and as an antiserum directed against group I CTXs has been shown to exhibit low cross-reactivity with group II CTXs (*8*), our result provides a likely explanation of the different immunogenecities between eastern and western cobra venom.

Despite the fact that severe gangrene and inflammation of skin are the most obvious symptoms of victims that survive cobra bites, there is little research about the detailed molecular mechanism. The suggestion that bacterial contamination of the wounded area is the major contributor of the effect lacks experimental support because there is no evidence for the presence of identifiable bacteria in large amounts or of a special type in the cobra fang (*57*). Since integrins, glycosaminoglycans, and its binding protein are known to be involved with wound healing and inflammation, it would be interesting to discover whether the establishment of CTX as a GAG- and integrin-binding toxin might help in understanding the CTX-induced severe tissue degeneration and inflammation. We point out that CTXs, although lacking RGD sequence, have recently been shown to bind to integrin $\alpha v\beta 3$ with decreasing specificity: CTX A5 > CTX A3 $\gg$ CTX A6 (*5*). Since the structural differences between CTX A6 and A3 (Table 1) are located mainly in the loop I region, our results also provide a structural explanation for the observed specificity of the CTX−integrin interaction.

Potential Targets of Group I CTXs As Revealed by Bioinformatics Analysis. Cyclolinopeptide A (CLA) is a naturally occurring cyclic nonapeptide isolated from linseed. The presence of a pair of cis-linked proline residues indicates that CLA might resemble cyclosporine or tacrolimus (FK 506, a macrolide lactone antibiotic) in targeting the cyclophilin or the peptidyl-prolyl *cis*−*trans*-isomerase (PPIases) family (*58*−*60*). CLA has been shown to mediate its immunosuppressive activity through cyclophilin-dependent calcineurin phosphatase inactivation (*61*). Moreover, an immunosuppressive drug of this type works mainly by blocking intracellular signaling pathways critical for the production of cytokines by lymphocytes. Considering that CTX can also be internalized into the cytoplasmic environment, an interesting hypothesis is to test whether group I CTXs can not only be conformational analogues of CLA but also find future application in understanding the mechanism of skin disorder.

We show in Figure 10 that a type VIa turn with a cis peptide bond between the two proline residues of CTX A6 is a dominant structural feature of the other well-characterized bioactive polypeptides of cyclolinopeptide A [cyclo-(Pro-Pro-Phe-Phe-Leu-Ile-Ile-Leu-Val)] and its analogues. Not only is a type VIa turn with both a cis Pro−Pro conformation and one to four hydrogen bond across the turn present for both compounds, but a similar conserved hydrophobic residue flanking the two prolines is also readily detectable. For instance, the two hydrophobic residues (Leu and Val) immediately preceding *cis*-Pro for CLA are substituted with well-conserved Leu and Ile residues, respectively. Similarly, the two hydrophobic residues (Phe and Phe) immediately following the second Pro for CLA are substituted with Phe and Trp, respectively (Tyr). As the conserved loop region of group I CTXs is fully exposed to the water environment and accessible to the interaction of other molecules, our results indicate that group I CTXs might share a similar molecular target with CLA.

Loop I of CTX A6 has a consensus sequence of PPxY known to interact with the class I WW domain. WW domains are the smallest, naturally occurring protein modules composed of approximately 40 amino acids. They are found in many different proteins and are implicated in several human

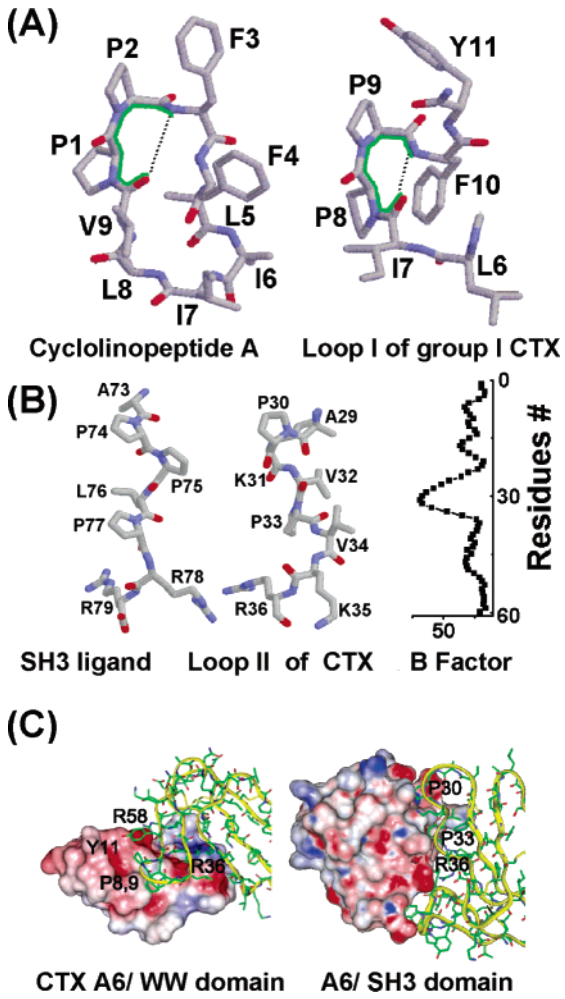

FIGURE 10: (A) Comparison of the conformation of cyclolinopeptide A and loop I of group I CTXs. Green and dotted lines represent the type VIa turn residues and the H-bond, respectively. (B) Comparison of the conformation of the SH3 domain-binding ligand and loop II of CTX. The right panel shows a plot of *B*-factor against amino acid residual positions of CTX A6. The amino acid residues with maximal *B*-factors are found to be located in the regions with the conserved sequence of the SH3 domain. (C) Models of the CTX A6−WW domain (left) and CTX A6−SH3 domain (right) complexes based on the structures of the dystrophin WW and *c-Src* SH3 domain. Molecular surfaces of WW and SH3 domains are colored as electrostatic potential with DelPhi, and CTX A6 is represented in stick and ribbon format.

diseases, such as Liddle's syndrome of hypertension, muscular dystrophy, Alzheimer's disease, and Huntington's disease. WW domains resemble SH3 domains functionally because of their affinity for proline-rich ligands. The SH3 domain mediates binding to proline-rich sequences with the minimum consensus residues of PxxP. Interestingly, with the availability of PxxPx+ class II ligand consensus sequence in CTX A6 at the functionally important loop II region, it is also a potential ligand for the SH3 domain (Figure 10B).

By using a computer docking method, we show in Figure 10C (left panel) that the cis conformation of loop I can indeed bind well to a WW domain (dystrophin). In the case of β-dystroglycan−dystrophin interaction, the hydroxyl group of tyrosine forms a hydrogen bond with His of dystrophin and ring stacking occurred between Pro of β-dystroglycan and Tyr of dystrophin. In the cis conformation of loop I, the Phe residue instead of Pro creates the ring stacking with Tyr of dystrophin. There are two additional interaction sites between CTX A6 and the WW domain. Arg58 and Arg36 of CTX A6 interact with the side chain of Glu72 and the carbonyl group of Ile65 of dystrophin, respectively.

A similar approach can also be studied to understand the interaction between group I CTXs and the SH3 binding domain (Figure 10C, right panel). The observed high *B*-factors for loop II of the CTX A6 crystal structure (Figure 10B, right panel) suggest that the conformation of CTX A6 near the tip of loop II is flexible. A simple reorientation of the Pro33 conformation at loop II of CTX A6 (Figure 10B, middle panel) immediately restores it to the conformation of the SH3-bound ligand. In fact, a computer docking experiment shows no serious steric hindrance between CTX A6 and the SH3 domain. We conclude that group I CTXs can indeed serve as potential ligands for Pro-rich ligands. A future experimental approach to test the hypothesis based on a molecular modeling approach would be interesting in determining whether a specific type of SH3 domain could serve as a specific biological target for its action. For instance, our preliminary binding study using a fluorescence spectroscopic method indicates that a weak interaction can be detected between CTX A6 and Grb2 (growth factor receptor-bound protein 2), but not between CTX A6 and BTK (Bruton's tyrosine kinase).

In summary, we present a three-dimensional X-ray crystal structure of a newly purified CTX A6 from the cobra venom of eastern Taiwan and show that its loop I conformation adopts a type VIa turn with a cis peptide bond located between two proline residues of PPxY. Comparative NMR and CD spectroscopic investigations reveal that such a conformation should prevail in all group I CTXs in both the solution and crystal state. Binding of group I CTXs to the membrane environment, however, induces a structural change of CTX with a new conformation similar to that of group II CTXs. Finally, the loop I conformation of group I CTXs sheds new light on identifying a potential protein target in understanding the action mechanism of CTX-induced severe tissue necrosis and inflammation.

ACKNOWLEDGMENT

We thank Yu-Cheng Jean, Yu-San Huang, Chun-Shiun Chao, and Chia-Ni Hsu for their technical assistance and discussion and the staff of the synchrotron radiation X-ray facility for data collection at BL17B2 of NSRRC in Taiwan, and Mau-Tsu Tang at BL12B2 of SPring-8 in Japan.

REFERENCES

1. Dufton, M. J., and Hider, R. C. (1991) The structure and pharmacology of elapid cytotoxins, in *Snake Toxins* (Harvey, A. L., Ed.) pp 259−298, Pergamon, New York.
2. Fletcher, J. E., Hubert, M., Wieland, S. J., Gong, Q. H., and Jiang, M. S. (1996) Similarities and differences in mechanisms of cardiotoxins, melittin and other myotoxins, *Toxicon 34*, 1301−1311.
3. Forouhar, F., Huang, W. N., Liu, J. H., Chien, K. Y., Wu, W., and Hsiao, C. D. (2003) Structural basis of membrane-induced cardiotoxin A3 oligomerization, *J. Biol. Chem. 278*, 21980−21988.
4. Hung, D. Z., Liau, M. Y., and Lin-Shiau, S. Y. (2003) The clinical significance of venom detection in patients of cobra snakebite, *Toxicon 41*, 409−415.
5. Wu, P. L., Mori, S., Lee, S. C., Akakura, N., Wu, W., and Takeda, Y. (2005) Specific binding of cobra cardiotoxins, members of the Ly-6 protein family, to integrin $\alpha v\beta 3$, *J. Biol. Chem.* (submitted for publication).

6. Chien, K. Y., Chiang, C. M., Hseu, Y. C., Vyas, A. A., Rule, G. S., and Wu, W. (1994) Two distinct types of cardiotoxin as revealed by the structure and activity relationship of their interaction with zwitterionic phospholipid dispersions, *J. Biol. Chem. 269*, 14473−14483.
7. Vyas, K. A., Patel, H. V., Vyas, A. A., and Wu, W. (1998) Glycosaminoglycans bind to homologous cardiotoxins with different specificity, *Biochemistry 37*, 4527−4534.
8. Grognet, J. M., Menez, A., Drake, A., Hayashi, K., Morrison, I. E., and Hider, R. C. (1988) Circular dichroic spectra of elapid cardiotoxins, *Eur. J. Biochem. 172*, 383−388.
9. O'Connell, J. F., Bougis, P. E., and Wüthrich, K. (1993) Determination of the nuclear-magnetic-resonance solution structure of cardiotoxin CTX IIb from *Naja mossambica mossambica*, *Eur. J. Biochem. 213*, 891−900.
10. Otting, G., Marchot, P., Bougis, P. E., Rochat, H., and Wüthrich, K. (1987) Monitoring the purification by high-performance liquid chromatography of cardiotoxins from *Naja mossambica mossambica* using phase-sensitive two-dimensional nuclear magnetic resonance, *Eur. J. Biochem. 168*, 603−607.
11. Bilwes, A., Rees, B., Moras, D., Menez, R., and Menez, A. (1994) X-ray structure at 1.55 Å of toxin γ, a cardiotoxin from *Naja nigricollis* venom. Crystal packing reveals a model for insertion into membranes, *J. Mol. Biol. 239*, 122−136.
12. Gilquin, B., Roumestand, C., Zinn-Justin, S., Menez, A., and Toma, F. (1993) Refined three-dimensional solution structure of a snake cardiotoxin: Analysis of the side-chain organization suggests the existence of a possible phospholipid binding site, *Biopolymers 33*, 1659−1675.
13. Jahnke, W., Mierke, D. F., Beress, L., and Kessler, H. (1994) Structure of cobra cardiotoxin CTX I as derived from nuclear magnetic resonance spectroscopy and distance geometry calculations, *J. Mol. Biol. 240*, 445−458.
14. Bhaskaran, R., Huang, C. C., Tsai, Y. C., Jayaraman, G., Chang, D. K., and Yu, C. (1994) Cardiotoxin II from Taiwan cobra venom, *Naja naja atra*. Structure in solution and comparison among homologous cardiotoxins, *J. Biol. Chem. 269*, 23500−23508.
15. Jang, J. Y., Krishnaswamy, T., Kumar, S., Jayaraman, G., Yang, P. W., and Yu, C. (1997) Comparison of the hemolytic activity and solution structures of two snake venom cardiotoxin analogues which only differ in their N-terminal amino acid, *Biochemistry 36*, 14635−14641.
16. Jayaraman, G., Kumar, T. K., Tsai, C. C., Srisailam, S., Chou, S. H., Ho, C. L., and Yu, C. (2000) Elucidation of the solution structure of cardiotoxin analogue V from the Taiwan cobra (*Naja naja atra*): Identification of structural features important for the lethal action of snake venom cardiotoxins, *Protein Sci. 9*, 637−646.
17. Rees, B., Bilwes, A., Samama, J. P., and Moras, D. (1990) Cardiotoxin VII4 from *Naja mossambica mossambica*. The refined crystal structure, *J. Mol. Biol. 214*, 281−297.
18. Dementieva, D. V., Bocharov, E. V., and Arseniev, A. S. (1999) Two forms of cytotoxin II (cardiotoxin) from *Naja naja oxiana* in aqueous solution: Spatial structures with tightly bound water molecules, *Eur. J. Biochem. 263*, 152−162.
19. Sue, S. C., Jarrell, H. C., Brisson, J. R., and Wu, W. (2001) Dynamic characterization of the water binding loop in the P-type cardiotoxin: Implication for the role of the bound water molecule, *Biochemistry 40*, 12782−12794.
20. Sun, Y. J., Wu, W., Chiang, C. M., Hsin, A. Y., and Hsiao, C. D. (1997) Crystal structure of cardiotoxin V from Taiwan cobra venom: pH-dependent conformational change and a novel membrane-binding motif identified in the three-finger loops of P-type cardiotoxin, *Biochemistry 36*, 2403−2413.
21. Singhal, A. K., Chien, K. Y., Wu, W., and Rule, G. S. (1993) Solution structure of cardiotoxin V from *Naja naja atra*, *Biochemistry 32*, 8036−8044.
22. Lin, S. R., Chang, L. S., and Chang, K. L. (2002) Separation and structure−function studies of Taiwan cobra cardiotoxins, *J. Protein Chem. 21*, 81−86.
23. Chang, L. S., Huang, H. B., and Lin, S. R. (2000) The multiplicity of cardiotoxins from *Naja naja atra* (Taiwan cobra) venom, *Toxicon 38*, 1065−1076.
24. Hung, C. C., Wu, S. H., and Chiou, S. H. (1993) Sequence characterization of cardiotoxins from Taiwan cobra: Isolation of a new isoform, *Biochem. Mol. Biol. Int. 31*, 1031−1040.
25. Saviano, M., Isernia, C., Rossi, F., Di Blasio, B., Iacovino, R., Mazzeo, M., Pedone, C., and Benedetti, E. (2000) Solid-state structural analysis of the cyclooctapeptide cyclo-(Pro1-Pro-Phe-Phe-Ac6c-Ile-D-Ala-Val8), *Biopolymers 53*, 189−199.
26. Di Blasio, B., Rossi, F., Benedetti, E., Pavone, V., Pedone, C., Temussi, P. A., Zanotti, G., and Tancredi, T. (1989) Bioactive peptides: Solid-state and solution conformation of cyclolinopeptide A, *J. Am. Chem. Soc. 111*, 9089−9098.
27. Gaymes, T. J., Cebrat, M., Siemion, I. Z., and Kay, J. E. (1997) Cyclolinopeptide A (CLA) mediates its immunosuppressive activity through cyclophilin-dependent calcineurin inactivation, *FEBS Lett. 418*, 224−227.
28. Mihalyi, E. (1968) Numerical values of the absorbances of the aromatic amino acids in acid, neutral, and alkaline solutions, *J. Chem. Eng. Data 13*, 179−182.
29. Lanzetta, P. A., Alvarez, L. J., Reinach, P. S., and Candia, O. A. (1979) An improved assay for nanomole amounts of inorganic phosphate, *Anal. Biochem. 100*, 95−97.
30. Jancarik, J., and Kim, S. H. (1991) Sparse matrix sampling: A screening method for crystallization of proteins, *J. Appl. Crystallogr. 24*, 409−411.
31. Otwinowski, Z., and Minor, W. (1997) Processing of X-ray diffraction data collected in oscillation mode, *Methods Enzymol. 276*, 307−326.
32. Matthews, B. W. (1968) Solvent content of protein crystals, *J. Mol. Biol. 33*, 491−497.
33. Rossmann, M. G. (1990) The molecular replacement method, *Acta Crystallogr. A46*, 24−31.
34. Brünger, A. T., Adams, P. D., Clore, G. M., DeLano, W. L., Gros, P., Grosse-Kunstleve, R. W., Jiang, J. S., Kuszewski, J., Nilges, N., Pannu, N. S., Read, R. J., Rice, L. M., Simonson, T., and Warren, G. L. (1998) Crystallography & NMR system: A new software suite for macromolecular structure determination, *Acta Crystallogr. D54*, 905−921.
35. Brünger, A. T. (1992) Free *R* value: A novel statistical quantity for assessing the accuracy of crystal structures, *Nature 355*, 472−475.
36. Jones, T. A., Zou, J. Y., Cowan, S. W., and Kjeldgaard, M. (1991) Improved methods for building protein models in electron density maps and the location of errors in these models, *Acta Crystallogr. A47*, 110−119.
37. Laskowski, R. A., MacArthur, M. W., Moss, D. S., and Thornton, J. M. (1993) PROCHECK: A program to check the stereochemical quality of protein structures, *J. Appl. Crystallogr. 26*, 283−291.
38. Engh, R. A., and Huber, R. (1991) Accurate bond and angle parameters for X-ray protein structure refinement, *Acta Crystallogr. A47*, 392−400.
39. Ramachandran, G. N., and Sasisekharan, V. (1968) Conformation of polypeptides and proteins, *Adv. Protein Chem. 23*, 283−438.
40. Wüthrich, K. (1986) in *NMR of proteins and nucleic acids*, John Wiley & Sons, New York.
41. Cavanagh, J., Fairbrother, W. J., Palmer, A. G., III, and Skelton, N. J. (1996) in *Protein NMR Spectroscopy*, Academic Press, New York.
42. Steinmetz, W. E., Bougis, P. E., Rochat, H., Redwine, O. D., Braun, W., and Wüthrich, K. (1988) ^{1}H nuclear-magnetic-resonance studies of the three-dimensional structure of the cardiotoxin CTXIIb from *Naja mossambica mossambica* in aqueous solution and comparison with the crystal structures of homologous toxins, *Eur. J. Biochem. 172*, 101−116.
43. Huang, X., Poy, F., Zhang, R., Joachimiak, A., Sudol, M., and Eck, M. J. (2000) Structure of a WW domain containing fragment of dystrophin in complex with β-dystroglycan, *Nat. Struct. Biol. 7*, 634−638.
44. Feng, S., Chen, J. K., Yu, H., Simon, J. A., and Schreiber, S. L. (1994) Two binding orientations for peptides to the Src SH3 domain: Development of a general model for SH3-ligand interactions, *Science 266*, 1241−1247.
45. Grishina, I. B., and Woody, R. W. (1994) Contributions of tryptophan side chains to the circular dichroism of globular proteins: Exiton couplets and coupled oscillators, *Faraday Discuss. 99*, 245−262.
46. Chakrabartty, A., Kortemme, T., Padmanabhan, S., and Baldwin, R. L. (1993) Aromatic side-chain contribution to far-ultraviolet circular dichroism of helical peptides and its effect on measurement of helix propensities, *Biochemistry 32*, 5560−5565.
47. Hider, R. C. (1988) An analysis of the 225−230-nm CD band of elapid toxins, *Biopolymers 27*, 113−122.
48. Sue, S. C., Brisson, J. R., Chang, S. C., Huang, W. N., Lee, S. C., Jarrell, H. C., and Wu, W. (2001) Structures of heparin-derived

disaccharide bound to cobra cardiotoxins: Context-dependent conformational change of heparin upon binding to the rigid core of the three-fingered toxin, *Biochemistry 40*, 10436−10446.
49. Jayaraman, G., Krishnaswamy, T., Kumar, S., and Yu, C. (1999) Binding of nucleotide triphosphates to cardiotoxin analogue II from the Taiwan cobra venom (*Naja naja atra*). Elucidation of the structural interactions in the dATP-cardiotoxin analogue II complex, *J. Biol. Chem. 274*, 17869−17875.
50. Richardson, J. S. (1981) The anatomy and taxonomy of protein structure, *Adv. Protein Chem. 34*, 167−339.
51. Tzeng, W. F., and Chen, Y. H. (1988) Suppression of snake-venom cardiotoxin-induced cardiomyocyte degeneration by blockage of Ca^{2+} influx or inhibition of non-lysosomal proteinases, *Biochem. J. 256*, 89−95.
52. Lin, S. R., Chang, K. L., and Chang, C. C. (1993) Chemical modification of amino groups in cardiotoxin III from Taiwan cobra (*Naja naja atra*) venom, *Biochem. Mol. Biol. Int. 31*, 175−184.
53. Schubert, M., Labudde, D., Oschkinat, H., and Schmieder, P. (2002) A software tool for the prediction of Xaa-Pro peptide bond conformations in proteins based on ^{13}C chemical shift statistics, *J. Biomol. NMR 24*, 149−154.
54. Efremov, R. G., Volynsky, P. E., Nolde, D. E., Dubovskii, P. V., and Arseniev, A. S. (2002) Interaction of cardiotoxins with membranes: A molecular modeling study, *Biophys. J. 83*, 144−153.
55. Chen, S. W., Huang, R. J., Chen, T. K., and Liau, M. Y. (1984) Comparison of the toxicity between east and west Taiwan cobra venoms, *Chin. Med. J. 34*, 644−649.
56. Daltry, J. C., Wuster, W., and Thorpe, R. S. (1996) Diet and snake venom evolution, *Nature 379*, 537−540.
57. Pongprasit, P., Mitrakul, C., and Noppakun, N. (1988) Histopathology and microbiological study of cobra bite wounds, *J. Med. Assoc. Thailand 71*, 475−480.
58. Howard, B. R., Vajdos, F. F., Li, S., Sundquist, W. I., and Hill, C. P. (2003) Structural insights into the catalytic mechanism of cyclophilin A, *Nat. Struct. Biol. 10*, 475−481.
59. Siemion, I. Z., Cebrat, M., and Wieczorek, Z. (1999) Cyclolinopeptides and their analogs: A new family of peptide immunosuppressants affecting the calcineurin system, *Arch. Immunol. Ther. Exp. 47*, 143−153.
60. Walsh, C. T., Zydowsky, L. D., and McKeon, F. D. (1992) Cyclosporin A, the cyclophilin class of peptidylprolyl isomerases, and blockade of T cell signal transduction, *J. Biol. Chem. 267*, 13115−13118.
61. Reynolds, N. J., and Al-Daraji, W. I. (2002) Calcineurin inhibitors and sirolimus: Mechanisms of action and applications in dermatology, *Clin. Exp. Dermatol. 27*, 555−561.

BI050172E